

Article

Effects of Ultrafine Blast Furnace Slag on the Microstructure and Chloride Transport in Cementitious Systems under Cyclic Drying–Wetting Conditions

Wei Li ¹, Liming Yi ¹, Wen Jiang ¹, Hua Dong ²  and Yong Zhang ^{3,*} 

¹ PowerChina Hubei Electric Engineering Co., Ltd., Wuhan 430040, China; liwsj@powerchina-hb.com (W.L.); yilmsj@powerchina-hb.com (L.Y.); jiangwsj@powerchina-hb.com (W.J.)

² Microlab, Section of Materials and Environment, Department of 3MD, Faculty of Civil Engineering and Geosciences, Delft University of Technology, 2628 CN Delft, The Netherlands; h.dong@tudelft.nl

³ College of Civil Engineering, Fuzhou University, Fuzhou 350116, China

* Correspondence: y.zhang@fzu.edu.cn

Abstract: This paper presents experimental investigations into the effects of ultrafine blast furnace slag on microstructure improvements against chloride penetration in saturated and unsaturated cementitious systems exposed to cyclic drying–wetting conditions. The hydration kinetics of ultrafine slag powders and pore solution chemistry in slag-blended cementitious systems at different ages, together with the main hydration products and pore structure characteristics, were determined. The chloride profiles accounting for different slag contents and drying–wetting cycles were measured. The results reveal that the reactivity of ultrafine slag can be well described with Avrami’s equation. The dilution effect of the slag predominated the pore solution chemistry, and the pH value decreased with a higher inclusion of slag. An optimal inclusion of 65% slag by mass of the binder corresponding to the finest pore structure and highest hydrotalcite content was found, which provides a reasonable basis for the slow chloride diffusion and high chloride binding. Under drying–wetting exposure, the specimen with a lower saturation exhibited a higher chloride transport caused by capillary absorption in the skin layer. The chloride transport tended to be diffusion controlled after sufficient drying–wetting cycles.

Keywords: ultrafine blast furnace slag; pore solution chemistry; microstructure; chloride transport; drying–wetting; unsaturated



Citation: Li, W.; Yi, L.; Jiang, W.; Dong, H.; Zhang, Y. Effects of Ultrafine Blast Furnace Slag on the Microstructure and Chloride Transport in Cementitious Systems under Cyclic Drying–Wetting Conditions. *Appl. Sci.* **2022**, *12*, 4064. <https://doi.org/10.3390/app12084064>

Academic Editors: Cesare Oliviero Rossi, Pietro Calandra, Paolino Caputo, Bagdat Teltayev, Valeria Loise and Michele Porto

Received: 28 March 2022

Accepted: 14 April 2022

Published: 18 April 2022

Publisher’s Note: MDPI stays neutral with regard to jurisdictional claims in published maps and institutional affiliations.



Copyright: © 2022 by the authors. Licensee MDPI, Basel, Switzerland. This article is an open access article distributed under the terms and conditions of the Creative Commons Attribution (CC BY) license (<https://creativecommons.org/licenses/by/4.0/>).

1. Introduction

The long-term behavior of reinforced concrete structures exposed to a tidal zone has been a serious concern in marine engineering [1]. Billions of dollars are annually required worldwide for maintenance purposes. A major cause of distress can be ascribed to the reinforcement corrosion induced by chloride attack. The soluble substances of cement create an alkaline nature, with a pH value close to 13 or above in the pore solution to passivate the steel surface. The accumulation of chloride ions on steel surfaces driven by persistent diffusion, together with capillary absorption in many situations, may destroy the passivity, resulting in steel corrosion. Chloride transport takes place through the microstructure of a cementitious system. Some of the chloride ions can be physically bound by the main hydration products C-S-H [2]. The alumina-rich AFm phases [3] consist of positively charged main layers $[\text{Ca}_2(\text{Al,Fe})(\text{OH})_6]^+$ and negatively charged interlayers $[\text{X.nH}_2\text{O}]^-$. They can chemically react with the chloride ions, forming the so-called Friedel’s salt. Chloride ions can be bound considerably by calcium oxychloride hydrate, which is formed in particular situations such as a high chloride concentration (3.5 mol/L) and low temperature (5 °C). Other phases, such as hydrotalcite, a representative of the layered

double hydroxides group, also play an important part in the adsorption of chlorides, especially for the concrete-containing ground granulated blast furnace slag [4].

The replacement of ordinary Portland cement OPC by ground granulated blast furnace slag, among others, at a large scale has become a common means for improved economic and sustainable considerations in marine concrete structures. The often-adopted cementitious slag has a relative density of around 2.9, and its particle fineness is usually higher than that of OPC. The use of slag has been shown to remarkably influence the initial particle packing and change the pore solution chemistry in cementitious systems. The hydration process and associated microstructure formation are expected to be quite different from those based on OPC. A practical question arises with respect to the current and future durability criteria when the slag is used as much as possible. A considerable number of scientific and engineering studies have been carried out over the past decades. The beneficial effects of slag utilization, particularly for chloride-laden environments, have always been a hot topic of research [5–13]. The role of slag in cementitious systems is affected by a variety of factors, such as chemical composition (CaO, MgO, Al₂O₃, and SiO₂), glass content, particle size distribution, etc. [14]. The enrichment of the SiO₂ is conducive to the pozzolanic reaction, a reason for the production of secondary C-S-H. The MgO of slag promotes the formation of hydrotalcite [15], contributing to chloride binding behavior. The Langmuir and Freundlich isotherms have been recognized in many cases as applicable for describing the relationship between the bound and free chlorides in cementitious systems [16].

A widespread consensus regarding the optimal inclusion level of slag with respect to maximizing the chloride resistance has not been reached yet. The common moderate dosage of 50% slag is adopted primarily according to strength considerations [17]. Thomas et al. [7] pointed out the time-dependent nature of chloride diffusion. They emphasized that the resistivity to chloride transport by adding slag is enhanced mainly for the periods after 6 months. This is partially related to the relatively slow hydration of slag. Field concretes are normally unsaturated, which plays a crucial role in long-term chloride transport. This issue has been highlighted and elaborated on in recent reports [10,11,18]. Based on a comprehensive literature survey, research on chloride penetration and transport mechanisms of unsaturated cementitious systems incorporating ultrafine slag powders are far from adequate. This is particularly true when the unsaturated specimens were exposed to the corrosive tidal zone of marine environments. All of this calls for the need for careful investigations to explore the fundamental aspects of slag addition on changes to microstructure-based transport properties under drying–wetting exposure.

The aim of the present work was to probe the hydration kinetics of ultrafine slag powders and to understand the microstructure characteristics of the hardened slag-blended cement paste specimens. The chloride transport properties of the corresponding mortar specimens under cyclic drying–wetting conditions were subsequently explored. The slag replacement level (0, 25, 65, and 85%) and degree of saturation (60, 80, and 100%) were considered in the mortar specimen preparation. The reactivity of slag with the hydration period was determined using the ethylene diamine tetraacetic acid (EDTA) dissolution method. The pore solution chemistry, including the concentrations of ions Na⁺, K⁺, and OH[−] as the hydration time elapsed, was figured out. Changes in the hydration products and pore structure with the inclusion of slag were characterized by means of thermogravimetric analysis TGA/DTG and mercury porosimetry, respectively. The chloride transport properties, with or without binding considerations, were measured. The effects of slag content, as well as the degree of saturation, on microstructure-based transport properties were emphasized and discussed in detail. The aim of this research is to help contractors and engineers make more reliable and sensible decisions for mixture designs using ultrafine blast furnace slag in marine concrete structures, in addition to more economic and sustainable concrete production.

2. Experimental Section

2.1. Raw Materials

P·O 42.5 Portland cement (OPC) and ground granulated blast furnace slag with a high fineness of 670 m²/kg were used. The main chemical compositions of the OPC and the slag as determined by X-ray fluorescence are shown in Table 1. The losses on ignition (LOIs) were 2.13 and 1.52 for the raw OPC and slag, respectively. It was expected that some carbonate compounds were included in both materials. The slag was mostly amorphous, with a minor crystalline phase of melilite, as evaluated by X-ray diffraction analysis. Paste and mortar samples were prepared using deionized water. The water to binder ratio (w/b) was kept constant at 0.42. Siliceous sand with particle sizes from 0.125 to 2 mm was used as the fine aggregate of the mortar samples. The mass ratio of the cement binder to sand was 1:3. The mortar samples were cured in a moist room with a temperature of 23 ± 2 °C and relative humidity above 98%. OPC was the essential part of all mixtures. The replacement levels of OPC by slag were 25, 65, and 85%. For each mixture, the hardened samples were cured for 1, 3, 7, 14, 28, 60, and 120 days. Three replicates of each mixture were prepared to ensure the reproducibility of the experimental data.

Table 1. Chemical composition of OPC and slag, weight %.

Items	OPC	Slag
CaO	64.32	41.52
SiO ₂	19.53	34.65
Al ₂ O ₃	4.67	11.12
Fe ₂ O ₃	3.45	0.53
MgO	1.98	8.12
K ₂ O	0.51	0.45
Na ₂ O	0.31	0.21
SO ₃	2.62	2.38
TiO ₂	0.32	1.05
LOI	2.13	1.52

2.2. Microstructure Characterization

A range of microstructural measurements was carried out on paste specimens of different ages. The reactivity of ultrafine slag particles and constitution of hydration products, as well as the pore solution chemistry and pore structure features, were determined to characterize the effects of slag addition on microstructure development.

The reaction of the ultrafine slag particles was explored based on the EDTA dissolution method, which enables the extraction of components other than unreacted slag. The EDTA residues are composed primarily of amorphous silica phases and also contain hydrotalcite phases as well. For correction purposes, EDTA extractions were performed on the neat OPC paste and raw slag powders. For details regarding the EDTA dissolution and data analysis, a reference can be made to the previous work of Lumley et al. [19]. The decomposition of the hydration products was traced from thermogravimetric analysis (TGA) using an STA (TG-DTA-DSC) 449 F3 Jupiter. The heating temperature was increased from 40 to 1000 °C with a heating rate of 10 °C/min. The weight loss of each component occurring at a particular temperature range was captured. The mass of the specimen used in the ceramic crucible was around 50 mg, and argon was used as the protective gas.

The pore solution of cylindrical paste specimens was collected according to the expression method proposed by Barneyback and Diamond [20]. The collected pore solution was stored in plastic bottles and sealed immediately to avoid water evaporation and carbonation. An inductively coupled plasma optical emission spectrometer was employed to quantify the pore solution chemistry. The concentrations of ions Na⁺, K⁺, Ca²⁺, and SO₄²⁻ were figured out. The concentration of OH⁻ and the pH value of the pore solution were determined based on titration against the 0.1 N HCl solution. In addition to hardened paste samples cured for 1~120 days, some paste samples, soon after casting at 2, 6, and 12 h, were

prepared, and the evolution of OH^- in the pore solution was measured. Changes in the OH^- at the very early stage were deemed as a reasonable index to trace the dissolution and hydration kinetics of slag particles.

Mercury intrusion porosimetry (MIP) was applied to assess the influences of ultrafine slag particles on the pore features of cementitious pastes. It was assumed that the cementitious pores were cylindrical and equally accessible to mercury. The relationship between the pore size and external pressure can be described using the well-known Washburn equation [21]. Prior to the MIP tests, the specimens at the desired age were immersed in liquid at $-195\text{ }^\circ\text{C}$ for 5 min and then moved to a freeze-dryer ($-24\text{ }^\circ\text{C}$ and 0.1 Pa) until a constant mass of the specimen was attained.

2.3. Chloride Penetration Measurements

Cylindrical mortar specimens $\Phi 100 \times 50$ mm cured for 120 days were used for chloride transport studies. These cylinders were formulated with different contents of slag. Before preconditioning, the mortar specimens of each mixture underwent a vacuum-saturation procedure. The saturated mortar specimens were then preconditioned at $50\text{ }^\circ\text{C}$ to different degrees of saturation, i.e., 60% and 80%. The partially saturated mortar specimens after the preconditioning were homogeneous in relative humidity. More details of the specimen treatment can be referred to in a previous report [22]. The degree of saturation of the mortar specimen can be determined using Equation (1).

$$S = \frac{m - m_d}{m_s - m_d}, \quad (1)$$

where S is the degree of saturation, m (g) is the mass of the sample at an unsaturated state, m_s (g) is the mass of the sample at a saturated state, and m_d (g) is the mass of the sample dried at $105\text{ }^\circ\text{C}$.

Chloride transport studies were carried out on mortar specimens exposed to cyclic drying–wetting conditions. All surfaces of the specimens were sealed except the tops, which were designed as the testing surfaces. The specimens at saturation levels of 100, 80, and 60% were placed in a climatic chamber maintained at $25 \pm 1\text{ }^\circ\text{C}$. The top surfaces of the mortar specimens were subjected to cyclic exposure of 6 h drying and 6 h wetting with a NaCl solution (165 g/L). Such a drying–wetting regime was adopted since it coincides with the exposure conditions for marine structures located in tidal zones. At the exposure periods of 2, 5, 10, 30, 50, and 70 drying–wetting cycles, the chloride profiles of the specimens were obtained by grinding powders layer-by-layer, together with potentiometric titration [23]. The (acid-soluble) total chloride profiles and (water-soluble) free chloride profiles were both measured [2,23,24]. The difference between the total and free chloride profiles represents the bound chloride profile. The chloride-binding isotherm for specimens of different slag content was analyzed. In the case of the diffusion of chloride ions in the specimen, the chloride transport can be quantitatively described based on the curve fittings of the chloride profile using the solution of Fick's second law, as shown in Equation (2).

$$c(x, t) = C_s - (C_s - C_i) \operatorname{erf} \left(\frac{x}{2\sqrt{D_a t}} \right), \quad (2)$$

where $c(x, t)$ is the total chloride content at depth x (m) after exposure time t (s); C_s is the surface chloride content; C_i is the initial chloride content of the material, which is zero in this work; D_a is the apparent chloride diffusion coefficient (m^2/s).

3. Results and Discussion

3.1. Hydration Kinetics of Slag-Blended System

The reacted and unreacted slag of the paste specimens at different ages were determined based on the EDTA dissolution method. The hydration degrees of the slag, defined as the ratio of the reacted slag over the total slag and as a function of age, are provided

in Figure 1. The three curves exhibit similar trends, regardless of the slag replacement level. In general, high reactivity of the ultrafine slag can be found and its hydration degree was above 21% for the paste specimen incorporating 25% slag, even on the first day of hydration. The rapid reaction of the slag proceeded until the end of 14 days. Afterwards, the slag continued to hydrate, but its reactivity seems to have decreased gradually. After 28 days, the hydration degree of the slag tended to be slowly increased as time elapsed. It is worthwhile to note that a higher slag content led to an obvious decrease in the hydration degree of slag. The content of calcium hydroxide CH, which acted as a necessary activator, largely controlled the reaction of the slag. The CH was produced in the process of the OPC hydration, and its content was lower for the specimens with a lower amount of OPC (namely, a higher amount of slag) in the binder mixture, as will be proved later in the present work.

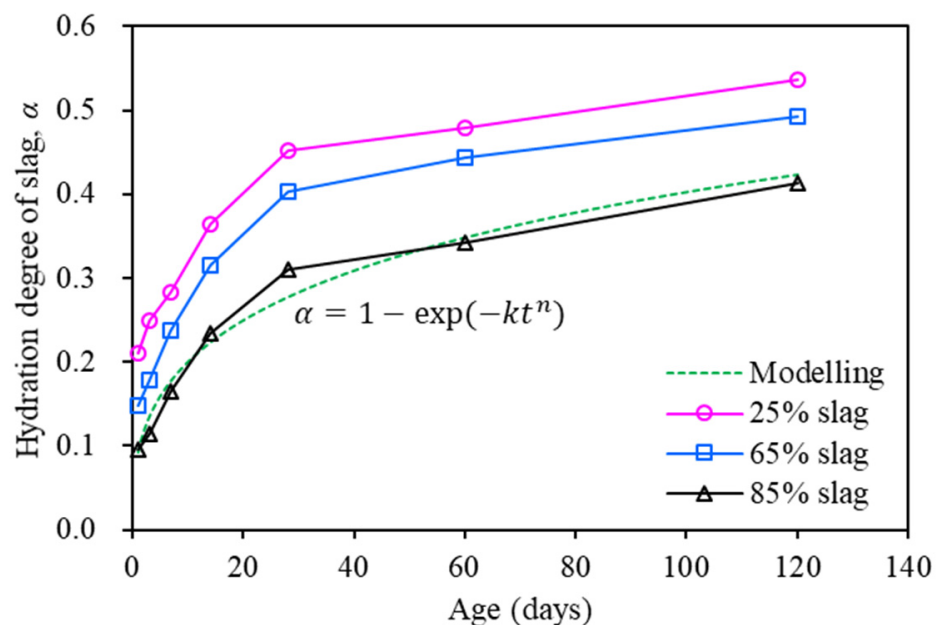


Figure 1. Hydration degree of ultrafine slag in paste specimens of different ages.

The hydration degree of slag as a function of age can be well described using Avrami's equation (Equation (3)), as referred to by Taylor [15]. The results by using Equation (3) to fit the experimental data of the 85% slag binder are shown as a green dotted line in Figure 1.

$$\alpha = 1 - \exp(-kt^n), \quad (3)$$

where α represents the hydration degree of the slag, and k and n are constants. The curve-fitting values of k and n , as well as the correlation coefficient R^2 , were derived and are given in Table 2.

Table 2. Values of fitting parameters in Avrami's equation.

Mixture	k	n	R^2
25% slag	0.22	0.27	0.97
65% slag	0.16	0.32	0.97
85% slag	0.10	0.36	0.98

The mass losses of various hydrates in the slag-blended paste specimens with elevated temperatures were quantified by TGA. The derivations (DTG) of the specimens at 28 days, as a representative result, are shown in Figure 2. The components are somewhat similar, as expected. A consistent mass loss of all specimens below 100 °C was observed, which partly resulted from the evaporation of free water and loosely bound water. The first main

peak at around 70 °C can be ascribed to the decomposition of ettringite (AFt). Losses of interlayer water in the main hydrates, C-S-H, took place at 50 °C. The dehydroxylation of C-S-H started at approximately 100 °C [15,25], and continuous loss of chemically bound water up to 800 °C was reported [26]. The decomposition in the temperature range of 140~400 °C is attributable to the series of AFm phases, which should include hemihydrate or monocarbonate, owing to the presence of CO_3^{2-} in the raw materials [27]. The two small peaks at about 300 °C and 380 °C can be related to the two-step dehydration of the lamellar hydrotalcite (Ht), which contains aluminum and magnesium [28].

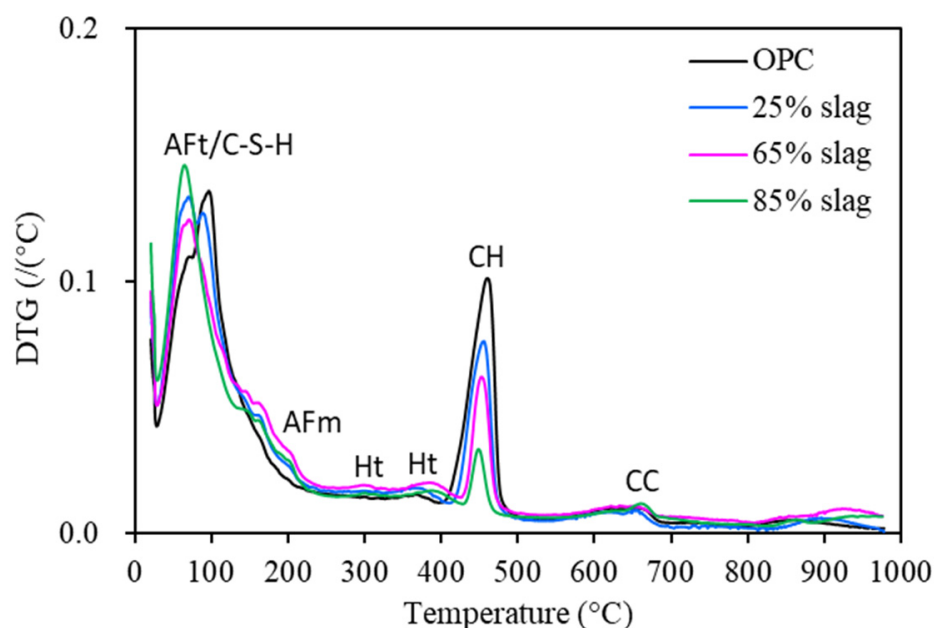


Figure 2. Differential thermogravimetric (DTG) curves of 28-day paste specimens incorporating different contents of slag: Aft—ettringite, Ht—hydrotalcite, CH—calcium hydroxide, CC—calcite.

The sharp peak between 400 and 500 °C corresponds to the dehydration of the crystal CH phase, followed by a small peak between 600 and 700 °C related to calcite (CC) decomposition. With quantitative analysis, it is clear that a higher AFt content was found when OPC was partially replaced by 25% slag, as seen in Figure 2. The AFt content decreased by increasing the substitution from 25 to 65%, while it increased again with a further rise in the replacement level by 85% slag. The CH content decreased with an increase in the slag content. The amounts of the alumina-rich AFm phases, as well as the Ht hydrates, are the highest for the 65% slag binder.

3.2. Pore Solution Chemistry

Figure 3 shows the results of the major ionic concentrations of the pore solutions expressed in paste specimens of increasing slag content hydrated from 1 day up to 120 days. The main components of the pore solutions were Na^+ , K^+ , and OH^- . The content of minor components Ca^{2+} and SO_4^{2-} were found to be obviously lower in the slag-blended binders than in the OPC binders. Their concentrations were below 0.01 mol/L for all slag-blended binders after 1 day. The data are not presented herein. It should be emphasized that logarithmic plots are presented in Figure 3c in order to observe more clearly the evolution of ions in the pore solution during the first few hours of mixing. Accordingly, very few changes in the OH^- can be seen in the first 6 h. It is expected that the concentrations of alkalis Na^+ and K^+ did not differ significantly in the meantime, considering the charge balance in the pore solution. Another expectation can be reached that the slag did not react in the first 6 h.

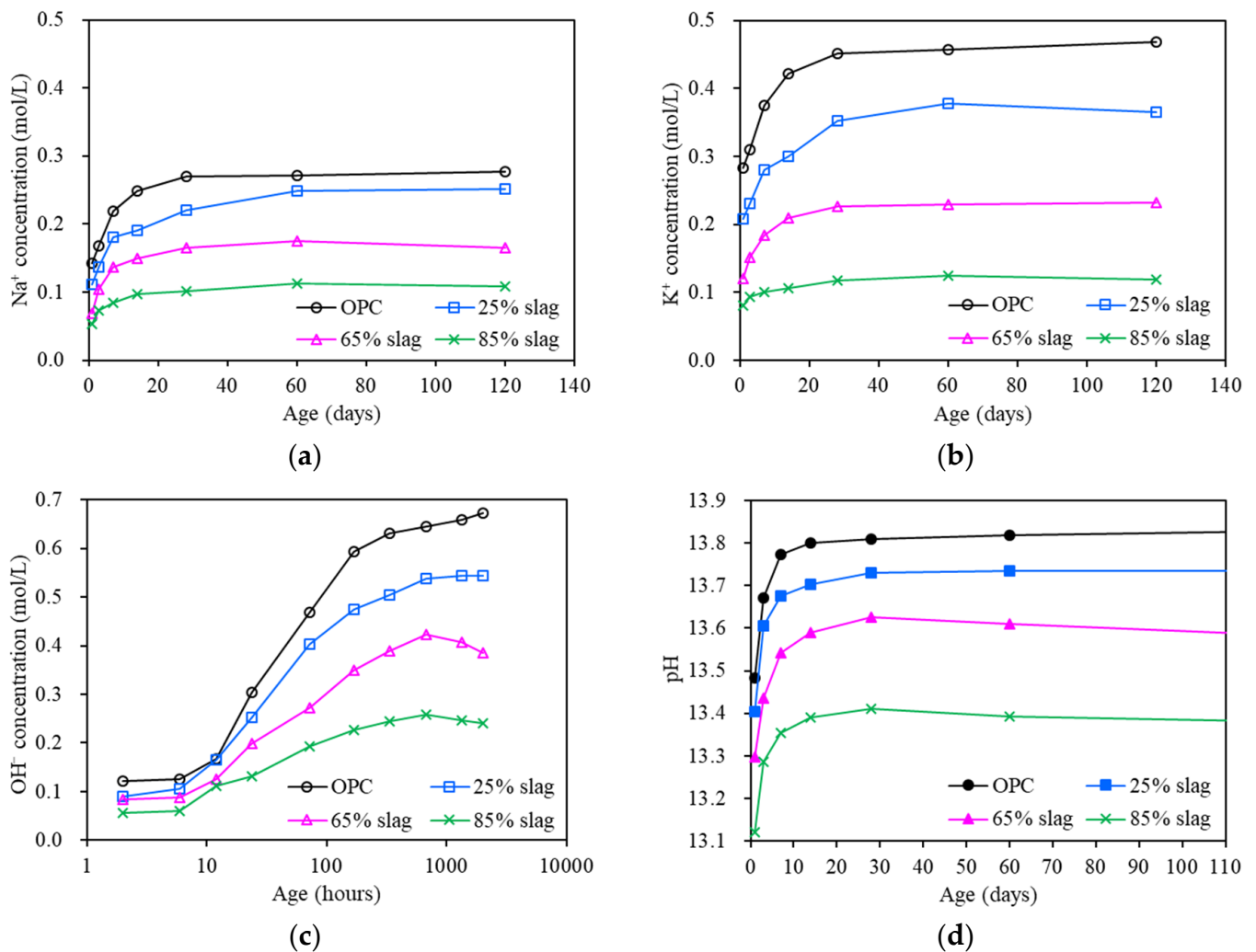


Figure 3. Concentrations of the main ions present in the pore solutions of OPC paste specimens with increasing slag contents: (a) Na^+ ; (b) K^+ ; (c) OH^- ; (d) pH value calculated based on OH^- concentration.

The addition of slag considerably changed the pore solution chemistry, particularly at later ages. A higher slag content normally results in lower concentrations of alkalis Na^+ and K^+ . The dilution effect of slag can be the main reason for the reduction of such ionic concentrations. Between 65% slag and 85% slag binders, the Na^+ concentration exhibited merely a slight difference at 1 day. However, the difference was apparently larger for the K^+ concentration. This implies that the alkalis in the raw slag particles had already dissolved in part. The dissolution of alkalis Na^+ and K^+ proceeded rapidly in the first 14 days. The ionic concentrations changed slowly after 28 days and tended to reach a plateau in the long term. This is true for both alkalis Na^+ and K^+ . On the other hand, a reduction in the ionic concentrations can be observed in some cases after 60 days, particularly for OH^- . This is related to the solubility of slag, which is limited at early ages and becomes pronounced at later ages. The continuous dissolution of slag leads to more hydration products (secondary C-S-H) to be precipitated in the capillary pores. These secondary C-S-H hydrates enable the adsorption of alkalis, subsequently reducing the alkali content in the pore solution.

The concentration of K^+ was obviously higher than that of Na^+ at all ages. At 1 day, the OH^- concentration decreased markedly from 0.30 mol/L of neat OPC binder to 0.13 mol/L of 85% slag binder. The difference in the OH^- concentration was further enlarged at the age of 120 days: 0.67 mol/L (OPC) versus 0.24 mol/L (85% slag). For all binders under study, the pH value differed in the range of 13.13~13.48 at 1 day, compared to 13.38~13.83 at

120 days. It is expected that all these binders with or without slag will maintain high alkalinity and keep high pH values in the long term.

3.3. Pore Structure

Characterizations of the pore structures in various paste specimens were carried out with MIP measurements. Figure 4 shows the results of the pore sizes for the 65% slag binder at the age of 1 day to 28 days. Two different pore categories, corresponding to the first and second peaks, are observed. The first peak represents the capillary pore system, which refers to the originally water-filled space, and the pore sizes were normally larger than 0.1 μm . The second peak represents the gel pore system, which was formed owing to the insufficient packing of hydration products. At 1 day, the amount of hydration products was limited and the majority of the pores belong to capillary pores. With the ongoing hydration process, more hydrates precipitated, filling the capillary pores and, as a result, the first peak is obviously smaller, while the second peak is larger, as can be reflected by the curve at 3 days. It seems that the first peak disappears after slag hydration of 7 days, and only one big bump relating to the gel pore system is observed. The bump moves towards the finer pore sizes as the hydration proceeds to 28 days.

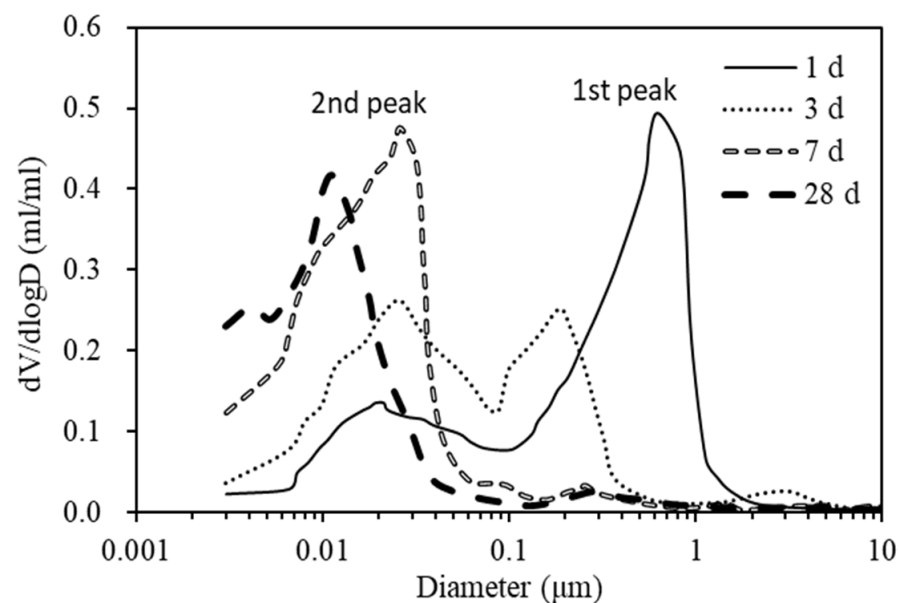


Figure 4. Evolution of pore sizes in the paste specimens adding 65% slag up to 28 days.

It is expected that capillary pores will always be present in hydrated cementitious systems [29]. The absence of the first peak for the specimens at later ages can be ascribed to the well-known ink-bottle effect [30]. The MIP technique assumes that all the pores are equally accessible to mercury. This assumption is surely inappropriate for cementitious systems [31], which have a wide range of pore sizes from the nano- to the micro-scale. During the MIP tests, the mercury intruded the throat (small) pores to reach the internal ink-bottle (large) pores. As a consequence, the first peak relating to the large pores cannot be precisely detected, in particular for the specimens with a dense microstructure.

Figure 5 compares the pore size distributions of 120-day paste specimens with increasing slag contents. The curve of each binder possesses one main peak. The pore size corresponding to the main peak is often noted as the critical pore diameter. It is normally considered that the critical pores, along with the pores larger than the critical pore diameter, are able to form a connected pore network, allowing for mass transfer. As such, the critical pore diameter plays a crucial role in mass transport properties. As indicated in Figure 5, the pore sizes turned out to be significantly finer with the addition of slag, irrespective of slag contents of 25~85%. The critical pore diameter dropped from 0.045 μm for OPC to 0.009 μm for 85% slag. The slag can react not only with calcium hydroxide but also with

water to produce calcium silicate hydrate C-S-H and calcium aluminates [32], leading to the densification of the microstructure. A higher replacement of OPC by slag from 25 to 65% tended to generate more C-S-H hydrates, leading to a remarkable pore structure refinement. This was, however, not the case when the slag replacement level further increased from 65 to 85%. The main reason can be related to the low content of CH in the 85% slag binder; therefore, it is difficult to fully activate the reactivity of the slag, as already proved in Figure 1.

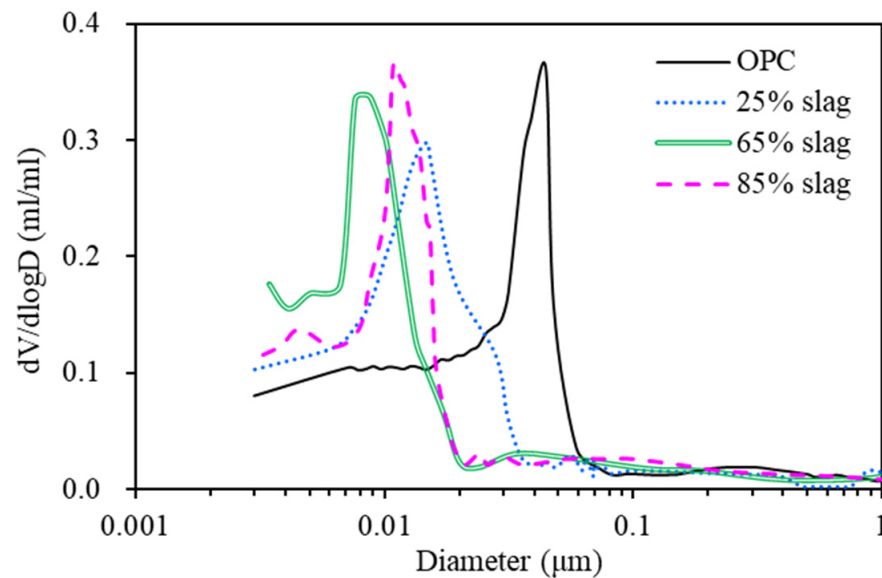


Figure 5. Pore size distributions of 120-day paste specimens with increasing slag content.

3.4. Chloride Transport Properties

Figure 6 shows the evolution of the total chloride profiles with drying–wetting cycles for 120-day saturated mortar specimens blended with 65% slag. Similar shapes are observed for all drying–wetting cycles. A common peak of chloride content is found in the outermost part of 3–4 mm. The chloride peak is closely related to the accumulation phenomenon caused by intermittent drying–wetting exposure. The drying procedure led to the evaporation of free capillary water, and the evaporation front moved inwards as time elapsed. Some chloride ions moved outwards along with the water evaporation, and others precipitated in the capillary pores due to oversaturation. In the subsequent wetting procedure, additional chlorides, along with an aqueous solution, were absorbed into the first layers of the specimen. The absorption front can normally reach the depth of the previous evaporation front, as the wetting process is significantly faster than the drying process. The amount of fluid evaporated after 8 days can be re-saturated by absorption within 2 h, as reported by Spraag et al. [33]. The chloride content corresponding to the peak increased clearly with the increase in the cycles. Saturation of the chloride content in the skin layer was not observed, even after 70 drying–wetting cycles, implying that the maximum chloride binding capacity was not reached. In the inner part of the specimen, the chloride content decreased with the depth and seems to have followed a diffusion-controlled process of ingress. This indicates that the convection caused by cyclic drying–wetting plays an important role in chloride penetration only in the first millimeters of slag-blended mortars.

Figure 7 displays the changes in the total chloride profiles in saturated mortar specimens of various slag contents after 10 drying–wetting cycles. The variation rule for the chloride content versus depth is basically the same, except that the chloride content was noticeably lower in the slag-blended binders than in the OPC binder. This observation is true for all different replacement levels of slag (25–85%). The 65% slag binder presented the lowest chloride content in the entire penetration depth. This can be intimately related to the

finest pore sizes in the microstructure of the 65% slag binder, as already addressed earlier. With an increase in the depth, the chloride content increased first and then decreased. This again proves the limited influential depth of drying–wetting cycles, known as the convection zone, on chloride penetration, irrespective of the binder type. The convection zone seems to be smaller when incorporating the slag. The main reason can be related to the much finer pore structure in the slag-blended binders, for which the evaporation front during the drying procedure is expected to be smaller than that in the OPC binder. The chloride peak formed within the convection zone was observed to be apparently higher for the OPC binder. The larger porosity and associated coarser pore sizes are considered to be in charge of the peak amplitude in the first 10 cycles of drying–wetting exposure. The large pores provided more space for the external chloride solution to penetrate into the surface part of the specimen.

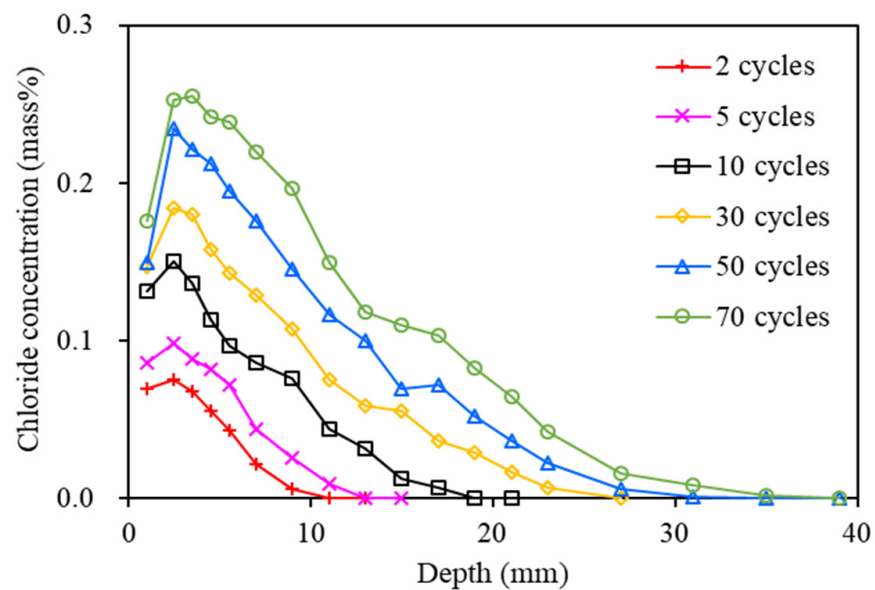


Figure 6. Effect of drying–wetting cycles on the total chloride profiles in 120-day saturated mortar specimens blended with 65% slag.

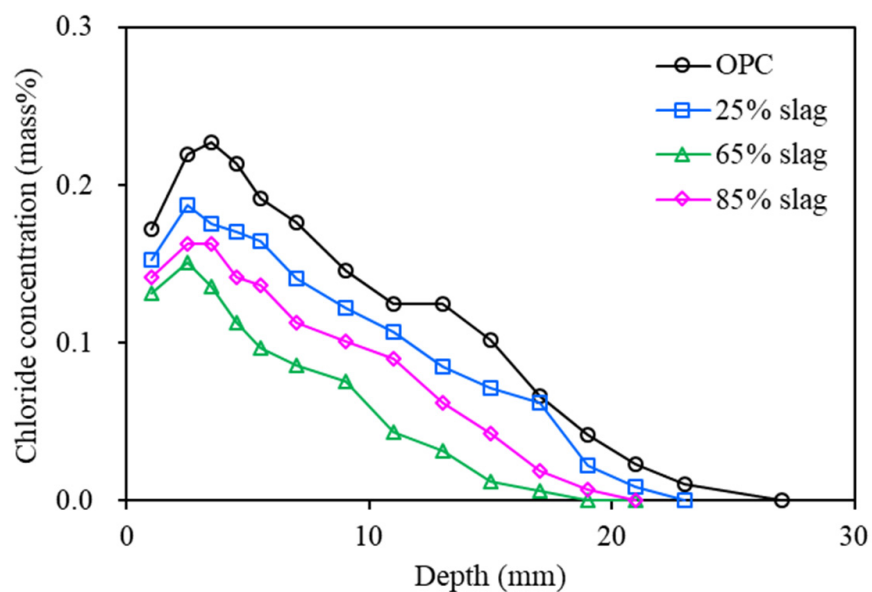


Figure 7. Effect of slag content on the total chloride profiles of saturated mortar specimens after 10 drying–wetting cycles.

Figure 8 depicts the differences in the total chloride profiles of mortar specimens in the saturated and unsaturated states. For saturated specimens ($S = 100\%$), there was a clear peak in the chloride content in the skin layer, and the peak became increasingly pronounced with the increasing drying–wetting cycles. For unsaturated specimens ($S = 60\%$), however, the accumulation of chlorides seems to have been less apparent, and the chloride peak disappeared in the outermost part of the specimen, in particular for the early drying–wetting cycles. The chloride content of the unsaturated specimens shows a slight decrease first and then a rapid drop with the depth. In the wetting process of the unsaturated specimens, capillary absorption predominated the transport phenomena, and the effect of capillary absorption seems to have been pronounced with the first increase in the drying–wetting cycles. As such, the chlorides could hardly be accumulated in the skin layer. On the other hand, the saturation level of the unsaturated specimen became higher with the continuous increase in the drying–wetting cycles, given that water evaporation caused by drying is much slower than water absorption caused by wetting. There may possibly be a critical saturation level, above which the influential depth of cyclic drying–wetting on chloride penetration tends to be decreased. The accumulation of chlorides in the skin layer of the unsaturated specimens ($S = 60\%$) could be observed after 50 drying–wetting cycles. For unsaturated specimens, the convection owing to cyclic drying–wetting played a significant role in the chloride penetration, and the chloride contents were considerably higher than those of the saturated specimens. This suggests that marine concrete in tidal zones should be cured with as much saturation as possible to avoid drastically rapid penetration of chloride at an early age of service.

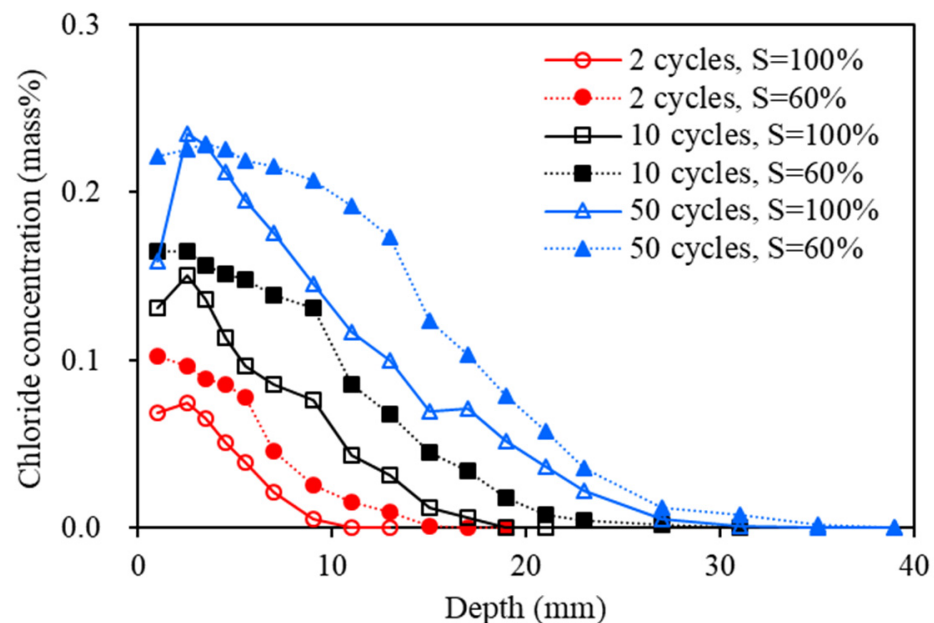


Figure 8. Total chloride profile of saturated ($S = 100\%$) and unsaturated ($S = 60\%$) mortar specimens.

To quantitatively describe the effect of drying–wetting cycles on chloride penetration, the experimental data of the total chloride profiles were fitted with Fick’s second law (Equation (2)). The apparent chloride diffusion coefficient D_a as a function of the drying–wetting cycles is displayed in Figure 9. It has been recognized that both capillary absorption and chloride diffusion influence the chloride penetration of specimens exposed to cyclic drying–wetting conditions. The D_a values given in Figure 9 were used primarily for comparative studies. The surface chloride content C_s does not have a consistent trend of change with increasing drying–wetting cycles according to the best-fit results using Equation (2). The D_a value, nevertheless, generally shows a decreasing trend with the increased cycles of drying–wetting exposure. A drastic drop in the D_a value can be seen at the early stages of the drying–wetting cycles, and a slightly slow decrease in the D_a value

was observed at later stages. The D_a value was considerably higher for the binders with lower saturation levels. The slag-blended binders exhibited markedly higher resistance to chloride penetration than the OPC binders, as reflected by the lower D_a values.

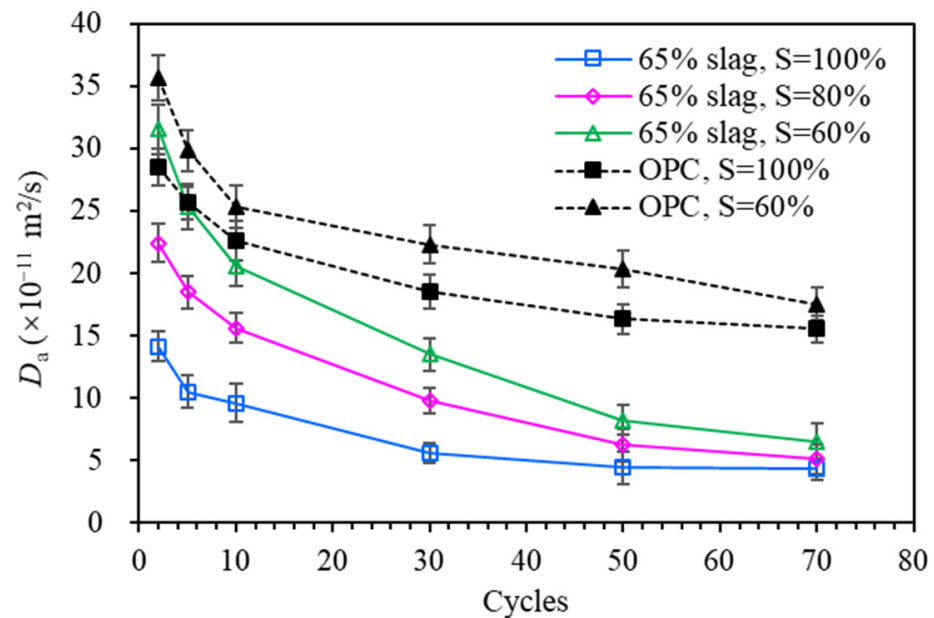


Figure 9. Apparent chloride diffusion coefficient D_a as a function of drying–wetting cycles for OPC and slag-blended mortars at different saturation levels.

It is interesting to note that the differences in the D_a values were diminished for 65% slag binders of various saturation levels. This was the same case for OPC binders. The D_a value may become quite similar for a particular binder even with a different initial saturation level after sufficient exposure to drying–wetting cycles. The chloride transport at early drying–wetting cycles, as indicated by the D_a value, seems to have been much more sensitive to the initial saturation level for the slag-blended binders than for the OPC binders. In the early days of drying–wetting exposure, capillary absorption played an important part in the chloride penetration of unsaturated binders. A lower saturation of the binder corresponded to higher capillary absorption, leading to a higher D_a value. The saturation level of unsaturated binders increased rapidly at the early exposure and then tended to increase gradually. As a consequence, the effect of drying–wetting cycles and the resultant capillary absorption of chloride penetration became less pronounced as the exposure continuously proceeded. Differences in the D_a values resulting from varying initial saturation levels decreased in the meantime. Between the binders of 65% slag and OPC at $S = 60\%$, their D_a values showed a small difference in the first cycles of exposure but a much larger difference after 70 cycles of exposure. This highlights the importance of the saturation level in the chloride penetration process. It should be kept in mind that the significantly positive effect of slag on the resistance to chloride penetration exists primarily when the materials are of high saturation levels. The role of saturation should be carefully taken into consideration in the case of pursuing a sufficient utilization of slag.

Figure 10 shows the relationship between bound chloride and free chloride in saturated mortar specimens with different replacement levels of slag after exposure to 70 drying–wetting cycles. The bound chloride content is expressed in mg/g after normalization to the mass of the mortar specimen. As observed, the slag-blended binders clearly had higher amounts of bound chloride than the neat OPC binder, in particular for the case of a high free chloride concentration. The 65% slag binder was found to have had the highest amount of bound chloride.

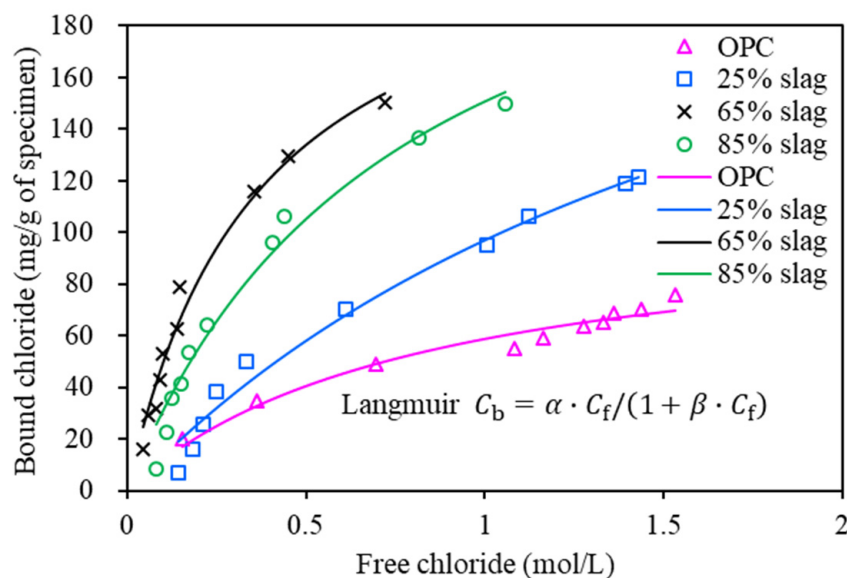


Figure 10. Chloride binding isotherm of saturated mortar specimens with increasing slag content after 70 drying–wetting cycles.

The increase in the chloride binding capacity by including slag is attributable in part to the formation of Friedel’s salt owing to a higher content of alumina in the raw slag materials. The dilution effects of slag addition on the concentrations of OH^- and SO_4^{2-} in the pore solution also played an important part in the higher binding of chlorides. Extensive completions between chloride, OH^- and SO_4^{2-} exist when reacting with alumina phases in cementitious systems. The presence of additional SO_4^{2-} reduces the binding of chlorides in both C-S-H and AFm phases in the sense that the C-S-H phases can include more SO_4^{2-} than chlorides [34]. A typical example related to this aspect can be found elsewhere [35]. A higher SO_4^{2-} content, in combination with aluminate-containing phases, leads to an increase in the tendency to transfer AFm to ettringite. A preferential reaction of sulfates with alumina-rich phases, such as AFm, was substantiated compared to the formation of chloride containing alumina phases, such as Friedel’s salts, as referred to in the work of Zibara [36]. The sites for chloride adsorbed on the main hydrates C-S-H are increased as soon as the content of OH^- is decreased. This has been well documented in previous works [37,38].

Another important aspect contributing to chloride binding is related to the significant refinement of the pore structure by incorporating slag. As described earlier in this work, the majority of pores are below 20 nm for slag-blended binders, compared to a coarser pore structure of OPC binder, with pore sizes mostly below 60 nm. The pore walls of hydrated cementitious systems are negatively charged, with a compact layer containing alkalis (Ca^{2+} , Na^+) and a diffuse layer adsorbed on the pore walls [39]. The presence of the electrical double layer enables the promotion of the chloride binding and, hence, delays the chloride penetration. It should also be mentioned that chloride can be adsorbed in the interlayer of hydrotalcite (Ht), a distinct hydration product from incorporating slag, and the interlayer space is then enlarged because of the larger sizes of the chloride ions compared to the hydroxide ions [40].

As abovementioned, a variety of factors contribute to the chloride binding behavior in the slag-blended binders. Clarification of the dominant factors influencing chloride binding is a topic of ongoing study and requires further in-depth investigation. With quantitative analysis, the relationship between bound chloride and free chloride shown in Figure 10 can be well described using the Langmuir isotherm, as shown in Equation (4). The correlation

coefficients from the curve fittings are all above 0.96. The difference in the slag content is the key reason for the variation in the chloride binding.

$$C_b = \alpha \cdot C_f / (1 + \beta \cdot C_f), \quad (4)$$

where C_b is the bound chloride content (%), C_f is the free chloride content (mol/L), and α and β are the fitting parameters.

4. Conclusions

The present work provides a comprehensive experimental study with respect to the effects of ultrafine blast furnace slag on hydration, microstructural formation, and chloride transport in cementitious specimens. The role of the degree of saturation in the resistance to chloride penetration is emphasized. The main conclusions can be summarized as follows.

- (1) The hydration kinetics of ultrafine slag powders can be well predicted using Avrami's equation. With increases in slag addition, the amount of calcium hydroxide was decreased while the ettringite content was found to be increased. The dilution effect dominated the pore solution chemistry. By adding 85% slag, the pH value decreased to a level below 13.4 and tended to be reduced slightly in the long term owing to the continuous hydration of the slag.
- (2) The lowest chloride penetrability was found by incorporating 65% slag, whereby the pore structure was significantly refined, delaying chloride diffusion. Meanwhile, the pore solution chemistry, including OH^- and SO_4^{2-} , was diluted, together with a high amount of hydrotalcite, promoting chloride binding. The effect of slag addition on chloride binding behavior agrees well with the Langmuir isotherm.
- (3) Under drying–wetting conditions, a chloride peak presented in the skin layer of saturated specimens, while the peak was not obvious for unsaturated specimens. The specimens of lower saturated levels exhibited a higher chloride transport at early exposure to drying–wetting cycles. The effect of the initial saturation level on chloride transport became less pronounced as the exposure continuously proceeded.
- (4) Between slag and OPC binders, the difference in the chloride transport driven by capillary action gradually diminished with a decrease in the saturation level. The use of slag greatly enabled the promotion of the resistance to chloride ingress under drying–wetting cycles, in particular for long-term exposure.

It is normally considered that higher fineness results in higher reactivity of slag powders. However, higher fineness will inevitably increase the amount of water needed to maintain fluidity, and slag powders react more drastically at an early age. Sudden hardening and cracking can then be expected in the cementitious system. A higher fineness of slag does not necessarily allow for a higher replacement level in cementitious systems. The hydration degree of slag tends to be decreased when more cement is replaced by slag, irrespective of the fineness. From a durability point of view, the hydration of slag to a higher degree should be emphasized when slag is used in marine concrete.

Author Contributions: Writing—original draft and investigation, W.L.; data curation and formal analysis, L.Y.; visualization and validation, W.J.; methodology and resources, H.D.; conceptualization, writing—review and editing and supervision, Y.Z. All authors have read and agreed to the published version of the manuscript.

Funding: This research was funded by the Key Laboratory of Advanced Civil Engineering Materials (Tongji University), Ministry of Education (202102), the Qishan Scholar (Overseas Program) of Fuzhou University (GXRC-19023), the Natural Science Foundation of Fujian Province, China (2020J01482), the National Natural Science Foundation of China (51903047), and the Natural Science Foundation of Jiangsu Province, China (BK20191270).

Institutional Review Board Statement: Not applicable.

Informed Consent Statement: Not applicable.

Data Availability Statement: The data presented in this study are available on request from the corresponding author.

Acknowledgments: The authors are grateful to the Fujian Provincial University Research Center for Advanced Civil Engineering Materials and the Microlab of Delft University of Technology. Both provided guidance and support for the present work.

Conflicts of Interest: The authors declare no conflict of interest.

References

1. Zhang, P.; Hou, D.S.; Liu, Q.; Liu, Z.L.; Yu, J. Water and chloride ions migration in porous cementitious materials: An experimental and molecular dynamics investigation. *Cem. Concr. Res.* **2017**, *102*, 161–174. [[CrossRef](#)]
2. Tang, L.P.; Nilsson, L.O. Chloride binding capacity and binding isotherms of OPC pastes and mortars. *Cem. Concr. Res.* **1993**, *23*, 247–253.
3. Baquerizo, L.G.; Matschei, T.; Scrivener, K.L.; Saeidpour, M.; Wadsö, L. Hydration states of AFm cement phases. *Cem. Concr. Res.* **2015**, *73*, 143–157. [[CrossRef](#)]
4. Kayali, O.; Khan, M.S.H.; Ahmed, M.S. The role of hydrotalcite in chloride binding and corrosion protection in concretes with ground granulated blast furnace slag. *Cem. Concr. Compos.* **2012**, *34*, 936–945. [[CrossRef](#)]
5. Dhir, R.K.; El-Mohr, M.A.K.; Dyer, T.D. Chloride binding in GGBS concrete. *Cem. Concr. Res.* **1996**, *26*, 1767–1773. [[CrossRef](#)]
6. Dehghanian, C.; Arjemandi, M. Influence of slag blended cement concrete on chloride diffusion rate. *Cem. Concr. Res.* **1997**, *27*, 937–945. [[CrossRef](#)]
7. Thomas, M.D.A.; Bamforth, P.B. Modelling chloride diffusion in concrete: Effect of fly ash and slag. *Cem. Concr. Res.* **1999**, *29*, 487–495. [[CrossRef](#)]
8. Yeau, K.Y.; Kim, E.K. An experimental study on corrosion resistance of concrete with ground granulate blast-furnace slag. *Cem. Concr. Res.* **2005**, *35*, 1391–1399. [[CrossRef](#)]
9. Otieno, M.; Beushausen, H.; Alexander, M. Effect of chemical composition of slag on chloride penetration resistance of concrete. *Cem. Concr. Compos.* **2014**, *46*, 56–64. [[CrossRef](#)]
10. Olsson, N.; Wahid, F.A.; Nilsson, L.O.; Thiel, C.; Wong, H.S.; Baroghel-Bouny, V. Wick action in mature mortars with binary cements containing slag or silica fume—The relation between chloride and moisture transport properties under non-saturated conditions. *Cem. Concr. Res.* **2018**, *111*, 94–103. [[CrossRef](#)]
11. Zhang, Y.; Yang, Z.X.; Ye, G. Dependence of unsaturated chloride diffusion on the pore structure in cementitious materials. *Cem. Concr. Res.* **2020**, *127*, 105919. [[CrossRef](#)]
12. Li, C.Z.; Song, X.B.; Jiang, L.H. A time-dependent chloride diffusion model for predicting initial corrosion time of reinforced concrete with slag addition. *Cem. Concr. Res.* **2021**, *145*, 106455. [[CrossRef](#)]
13. Hu, X.; Poon, C.S. Chloride-related steel corrosion initiation in cement paste prepared with the incorporation of blast-furnace slag. *Cem. Concr. Compos.* **2022**, *126*, 104349. [[CrossRef](#)]
14. Escalante, J.I.; Gomez, L.Y.; Johal, K.K.; Mendoza, G.; Mancha, H.; Mendez, J. Reactivity of blast furnace slag in Portland cement blends hydrated under different conditions. *Cem. Concr. Res.* **2001**, *31*, 1403–1409. [[CrossRef](#)]
15. Taylor, H.F.W. *Cement Chemistry*; Thomas Telford: London, UK, 1997; p. 480.
16. Glass, G.K.; Hassanein, N.M.; Buenfeld, N.R. Neural network modelling of chloride binding. *Mag. Concr. Res.* **1997**, *49*, 323–335. [[CrossRef](#)]
17. Mackechnie, J.R.; Alexander, M.G.; Jaufeerally, H. *Structural and Durability Properties of Concrete Made with Corex Slag*; University of Cape Town: Cape Town, South Africa, 2003.
18. Zhang, Y.; Ye, G.; Yang, Z.X. New insights into long-term chloride transport in unsaturated cementitious materials: Role of degree of water saturation. *Constr. Build. Mater.* **2020**, *238*, 117677. [[CrossRef](#)]
19. Lumley, J.S.; Gollop, R.S.; Moir, G.K.; Taylor, H.F.W. Degrees of reaction of the slag in some blends with Portland cements. *Cem. Concr. Res.* **1996**, *26*, 139–151. [[CrossRef](#)]
20. Barneyback, R.S.; Diamond, S. Expression and analysis of pore fluids from hardened cement pastes and mortars. *Cem. Concr. Res.* **1981**, *11*, 279–285. [[CrossRef](#)]
21. Washburn, E.W. Note on a method of determining the distribution of pore sizes in a porous material. *Proc. Natl. Acad. Sci. USA* **1921**, *7*, 115–116. [[CrossRef](#)]
22. Zhang, Y.; Zhang, M.Z.; Ye, G. Influence of moisture condition on chloride diffusion in partially saturated ordinary Portland cement mortar. *Mater. Struct.* **2018**, *51*, 36. [[CrossRef](#)]
23. Climent, M.A.; Viqueira, E.; De Vera, G.; López-Atalaya, M.M. Analysis of acid-soluble chloride in cement, mortar, and concrete by potentiometric titration without filtration steps. *Cem. Concr. Res.* **1999**, *29*, 893–898. [[CrossRef](#)]
24. Chaussadent, T.; Arliguie, G. AFREM test procedures concerning chlorides in concrete: Extraction and titration methods. *Mater. Struct.* **1999**, *32*, 230–234. [[CrossRef](#)]
25. Gallé, C. Effect of drying on cement based materials pore structure as identified by mercury intrusion porosimetry—A comparative study between oven, vacuum and freeze drying. *Cem. Concr. Res.* **2001**, *31*, 1467–1477. [[CrossRef](#)]

26. Scrivener, K.; Snellings, R.; Lothenbach, B. *A Practical Guide to Microstructural Analysis of Cementitious Materials*; CRC Press: Boca Raton, FL, USA; Taylor & Francis Group: Boca Raton, FL, USA, 2016.
27. Kuzel, H.J.; Pollmann, H. Hydration of C_3A in the presence of $Ca(OH)_2$, $CaSO_4 \cdot 2H_2O$ and $CaCO_3$. *Cem. Concr. Res.* **1991**, *21*, 885–895. [[CrossRef](#)]
28. Lothenbach, B.; Durdzinski, P.; De Weerd, K. Thermogravimetric analysis. In *A Practical Guide to Microstructural Analysis of Cementitious Materials*; Scrivener, K.L., Snellings, R., Lothenbach, B., Eds.; CRC Press: Boca Raton, FL, USA; Taylor & Francis Group: Boca Raton, FL, USA, 2015; pp. 177–211.
29. Powers, T.C. Physical properties of cement paste. In Proceedings of the 4th ISCC, Brussels, Belgium, 5 February 2014; National Bureau of Standards: Washington DC, USA, 1960; Volume 2, pp. 577–613.
30. Zhang, Y.; Yang, Z.X.; Ye, G. Distribution of the ink-bottle pores in cementitious materials identified by intrusion-extrusion cyclic mercury porosimetry. *Unpublished work*.
31. Diamond, S. Mercury porosimetry: An inappropriate method for the measurement of pore size distributions in cement-based materials. *Cem. Concr. Res.* **2000**, *30*, 1517–1525. [[CrossRef](#)]
32. Jaul, W.C.; Tsay, D.S. A study of the basic engineering properties of slag cement concrete and its resistance to seawater corrosion. *Cem. Concr. Res.* **1998**, *28*, 1363–1371.
33. Spragg, R.P.; Castro, J.; Li, W.; Pour-Ghaz, M.; Huang, P.T.; Weiss, J. Wetting and drying of concrete using aqueous solutions containing deicing salts. *Cem. Concr. Compos.* **2011**, *33*, 535–542. [[CrossRef](#)]
34. De Weerd, K.; Orsáková, D.; Geiker, M.R. The impact of sulphate and magnesium on chloride binding in Portland cement paste. *Cem. Concr. Res.* **2014**, *65*, 30–40. [[CrossRef](#)]
35. Wowra, O.; Setzer, M.J. Sorption of chlorides on hydrates cement and C_3S pastes. In *Frost Resistance of Concrete*; Setzer, M.J., Auberg, R., Eds.; E & FN Spon: London, UK, 1997; pp. 147–153.
36. Zibara, H. Binding of External Chlorides by Cement Paste. Ph.D. Thesis, Department of Civil Engineering, University of Toronto, National Library of Canada, Ottawa, ON, Canada, 2001.
37. Glasser, F.P.; Kindness, A.; Stronach, S.A. Stability and solubility relationships in AFm phases: Part, I. Chloride, sulfate and hydroxide. *Cem. Concr. Res.* **1999**, *29*, 861–866. [[CrossRef](#)]
38. Jain, A.; Gencturk, B.; Pirbazari, M.; Dawood, M.; Belarbi, A.; Sohail, M.G.; Kahraman, R. Influence of pH on chloride binding isotherms for cement paste and its components. *Cem. Concr. Res.* **2021**, *143*, 106378. [[CrossRef](#)]
39. Chatterji, S.; Kawamura, M. Electrical double layer, ion transport and reactions in hardened cement paste. *Cem. Concr. Res.* **1992**, *22*, 774–782. [[CrossRef](#)]
40. Ke, X.; Bernal, S.A.; Provis, J.L. Uptake of chloride and carbonate by Mg-Al and Ca-Al layered double hydroxides in simulated pore solutions of alkali-activated slag cement. *Cem. Concr. Res.* **2017**, *100*, 1–13. [[CrossRef](#)]